NUCL SCI TECH (2019) 30:181
https://doi.org/10.1007/s41365-019-0707-y

Gas-cooled thorium reactor at various fuel loadings and its modification by a plasma source of extra neutrons

Andrey Arzhannikov[1] · Sergey Bedenko[2] · Vladimir Shmakov[3] · Vladimir Knyshev[2] · Igor Lutsik[2] · Vadim Prikhodko[1] · Igor Shamanin[2]

Received: 13 May 2019 / Revised: 25 July 2019 / Accepted: 28 July 2019 / Published online: 20 November 2019

Abstract This work presents the results of computer simulation of neutronic processes in a high-temperature gas-cooled thorium reactor for 30 different options of core loading. To guarantee stable and long-term reactor operation (7–10 years), the quantity of fuel compact dispersion phase and starting fuel composition was selected. It is demonstrated that it is possible in principle to substitute the near-axial recirculation zone of the reactor core by a long magnetic trap with a high-temperature plasma column for generating thermonuclear neutrons. The distribution of neutron yield along the length of the plasma source is also presented. Such a thorium reactor, with a near-axial source of extra neutrons, can be applied for researching thermophysical and neutronic characteristics of dispersion thorium fuel to improve its properties. The results of the work are of great interest from the perspective of future advancement of the thermonuclear power industry, by means of creation of a hybrid installation based on a thorium reactor with a long plasma column as a source of additional neutrons.

This work was supported by RFBR, project number 19-29-02005 mk.

✉ Sergey Bedenko
bedenko@tpu.ru

[1] Budker Institute of Nuclear Physics SB RAS, Novosibirsk, Russia 630090

[2] National Research Tomsk Polytechnic University, Tomsk, Russia 634050

[3] Russian Federal Nuclear Center–Zababakhin Institute of Applied Physics, Snezhinsk, Russia 456770

Keywords Low-power thorium reactor · Thorium hybrid reactor · Nuclear fuel evolution

1 Introduction

The study of the physics of low-power high-temperature gas-cooled thorium reactor units (HGTRU) (Tomsk Polytechnic University (TPU), Tomsk) was started 3 years ago [1–3], and its authors have already chosen the most appropriate core configuration and nuclear fuel material composition. The authors have stated [1] that the reactor being studied is capable of operating for no less than 3000 effective days at a power of 60 MWth.

Reactors of this type [1–18] are considered ideal sources of energy and heat for supplying power to distant regions of the country and do not require large reservoirs or rivers. In case of bringing such reactors [1, 2, 8–18] to a commercially competitive level, they are intended to ensure the power industry basis of such Russian regions. These reactors have several advantages in comparison with other types: high reliability, high efficiency (up to 50%), possibility to use fuel of different types and compositions, short period of construction and equipment delivery, low cost (in comparison with the thermal light-water reactors (LWR) generally used and the BN-type (BN-600, -800) sodium-cooled fast breeder reactor), and simplified management of spent fuel.

A special feature of the reactor studied in this work [1, 2] is that it is able to produce heat, electricity, and hydrogen simultaneously, and its core can easily be modified for solving another task [19]. In addition, the reactor power can be adjusted according to regional energy needs.

At present, a series of experiments is being carried out at TPU for the purpose of studying the physical properties of new-generation nuclear fuel for HGTRU. Dispersion fuel, which is being developed at TPU, is also a new-generation fuel. It is a fuel material with advanced mechanical, thermophysical, and neutronic properties. As the reactor core has not previously been studied with this fuel in neutronic experiments, it was necessary to create an installation to carry out the required experiments. A special facility intended for studying the neutronic properties of the dispersion (Th, Pu)O_2 fuel was suggested in the capacity of such installation by the employee group of Budker Institute of Nuclear Physics of SB RAS (Novosibirsk, Russia) [19]. This facility is an assembly of fuel blocks, the axial part of which is substituted by a long magnetic trap [20, 21] with high-temperature plasma providing generation of thermonuclear neutrons.

The results of computer simulation of neutronic processes in the core of the HGTRU for 30 different loading options are presented in the paper.

To ensure stable reactor operation, the fraction of the dispersion phase and the composition of the starting fissionable nuclide were chosen. The possibility to modify the axial part of the core was investigated in accordance with the concept suggested in the works [19]. From the perspective of advancement in the field of fundamental knowledge, the purpose of these researches is to expand and to deepen understanding of the possibilities that are opening up due to the development of thermonuclear energy technologies of the future. From the perspective of solutions to important applied tasks, it can be said that the results will form the basis of organizing the stable operation of HGTRU in a long-term operating cycle (no less than 7 years), with a high burn-up degree of both the thorium and plutonium components of the fuel.

2 Numerical investigation

2.1 Computational model of the basic core configuration

The core of the HTGRU (red colored area in Fig. 1, see [1]) consists of fuel blocks in the configuration of graphite hexagons. The core is surrounded by two rows of graphite hexagons of the same configuration, but without holes for fuel (white colored area in Fig. 1). On the top and bottom, the core is also closed with graphite blocks, but here they are laid in just one row.

Schematic drawings of the fuel block and its cross-section are presented in Fig. 2. One can see that there are cylindrical channels along the length of the block. The fuel block contains 76 channels of small diameter for fuel

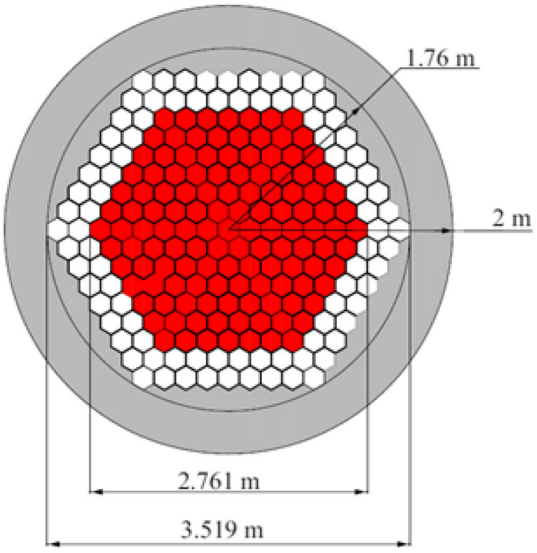

Fig. 1 Schematic of the cross-section of a reactor core model (Color online)

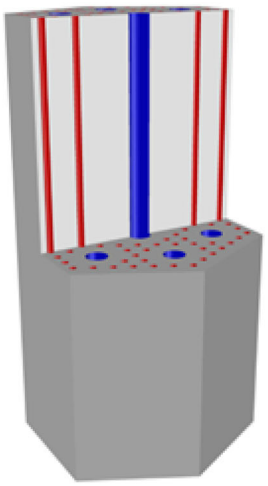

(a)

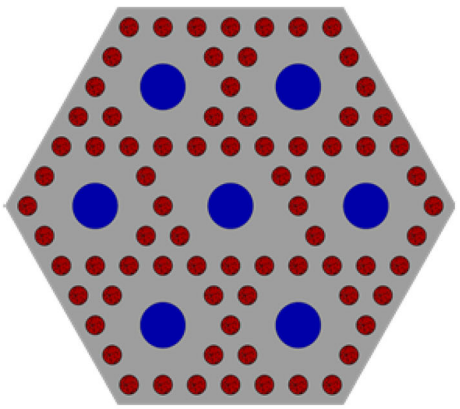

(b)

Fig. 2 Schematics of the core fuel block (**a**) and its cross-section (**b**) (Color online)

pellets (indicated in red) and seven channels of large diameter for helium flows (indicated in blue). The width of the graphite fuel block is 0.207 m, and its height is 0.8 m. The width of the graphite block enclosing the core at both the top and bottom is also 0.207 m, but its height is 0.3 m.

Microencapsulated fuel (microfuel) for a fuel pellet of HGTRU (Fig. 3, [1]) is a spherical fuel kernel of fissionable material (Th, Pu)O_2 with a diameter of 350 μm, covered successively by layers of pyrolytic carbon (PyC) and Ti_3SiC_2. These fuel kernels are dispersed into a graphite matrix of cylindrical fuel pellets (Fig. 3), which are placed in the fuel block.

At the first stage of research presented in the works [1–3], three types of fuel pellets with reference designations 0817, 1017, and 1200 were used. The diameters of these fuel pellet types were different: 8.17×10^{-3}, 10.17×10^{-3}, and 12.00×10^{-3} m, respectively. The heights of the fuel pellets (20×10^{-3} m) and thicknesses of the external SiC layer (0.3×10^{-3} m) were equal for all types. The percentage of heavy metal content in all types of fuel pellets were (%): Pu–50, ^{232}Th–50; and the isotopic compositions of Pu were (wt%) [1]: 238–0, 239–94, 240–5.4, 241–0.6, 242–0.

In the work [1], it is shown that an increase in fuel pellet diameter leads to a decrease in the initial excess of reactivity ρ_{inf} ($\rho_{inf} = (k_{inf} - 1)/k_{inf}$) (providing the size dimensions of the reactor fuel block are unchanged).

It should be noted that the reactor operation time depends on the initial quantity of Pu, Th in the loaded fuel and accumulated isotopes ^{241}Pu and ^{233}U.

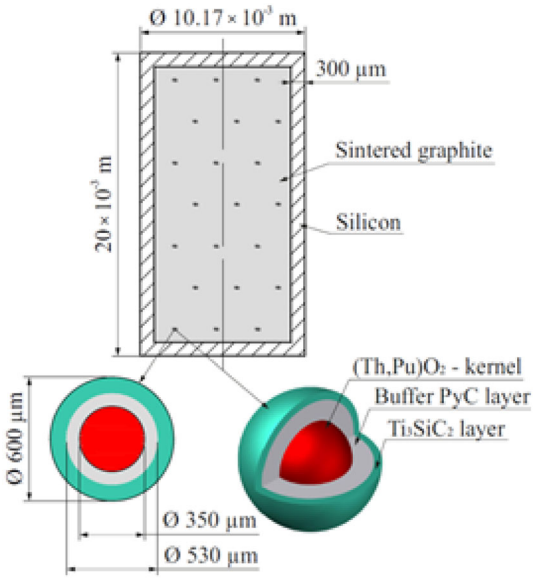

Fig. 3 Microencapsulated fuel and fuel pellet of the type 1017 (Color online)

When a fuel pellet of the type 0817 is used, the isotope ^{239}Pu burns up quickly and the secondary fuel (^{241}Pu and ^{233}U) does not manage to accumulate in quantities sufficient for stable and long-term operation of the reactor.

Therefore, after 1250 days of reactor operation, there is too little ^{239}Pu left in the core (less than 2%), and ρ_{inf} sharply falls to 0. When the fuel pellets of the types 1017 ($d\rho_{inf}/dt \approx 0.011$ %/days) and 1200 ($d\rho_{inf}/dt \approx 0.007$ %/days) are used, it results in the accumulation of ^{233}U, ^{241}Pu in the middle of the fuel cycle, prolonging the core life with steadier reactor operation.

It should be noted that for pellets of the type 0817, 1017, and 1200, the burn-up of ^{239}Pu ($\eta(^{239}\text{Pu}) = (N(t_{beginning}) - N(t_{end}))/N(t_{beginning})$) is 95.5, 96.6 and 92.7%, respectively [1]. This means that loading the core with type 1200 fuel pellets is the most appropriate for achieving maximum fuel core lifetime.

Further calculations showed (Fig. 4) that an increase in the dispersed phase fraction ω_f ($\omega_f = V_{microfuel} \times N/V_{matrix}$) of the type 1200 fuel pellet results in a decrease in $\eta(^{239}\text{Pu})$. Consequently, to provide better burn-up of ^{239}Pu in the (Th, Pu)-fuel cycle, the type 1017 fuel pellet has to be chosen.

Computations were performed for the unit cell of the infinite regular lattice (k_{inf}) in the program WIMS-D5B; the fuel part of the cell was homogenized. The computational model of the cell unit is presented in [1]; the homogenization process is described in the works [1, 22]. WIMS-D5B (Nuclear Energy Agency) is a universal program for computing cells of different reactor types. The WIMS code uses a 69-group system of constants on the basis of the evaluated nuclear database ENDF/B-VII.0 (the basic library has been compiled with 14 fast groups, 13 resonance groups, and 42 thermal groups), which allows computing in reactors of fast and thermal neutrons. In

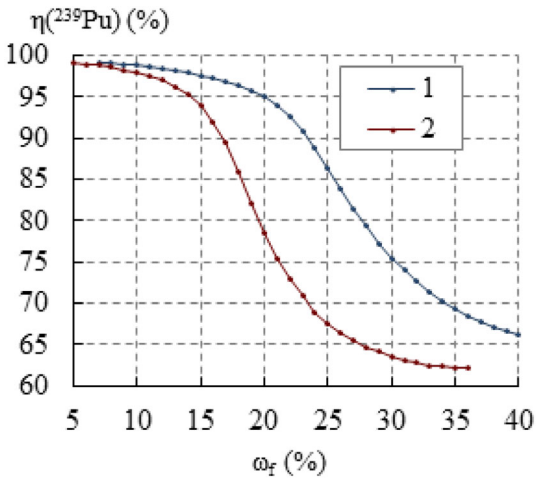

Fig. 4 Neutronic properties of the reactor cell unit for two types of fuel pellet: 1—type 1017; 2—type 1200 (Color online)

WIMS, the accuracy of the computed functionals is set by the step equal to 10 days. To assess poisoning in the reactor by xenon, the first 2 days are computed separately.

2.2 Neutronic computations for different core-loading configurations

At the second stage of the performed computer calculations, the cylindrical reactor cell that is an equivalent of the Wigner–Seitz system is studied. The fuel part of the cell is homogenized; computations are also performed in the program WIMS-D5B. To determine the effective *K*-factor (k_{eff}), an axial and radial geometrical parameter (B) is introduced. It is computed considering the transition from the actual core size to the equivalent Wigner–Seitz system. "White mirror" is used as a boundary condition on the side surface of the cell, and "translation symmetry" is used on the cell faces. The computation results of 30 core-loading options with type 1017 fuel pellets are presented in Fig. 5.

The results of the computer simulation show that the increase in ω_{f} after reaching a level of 17–18% does not lead to any noticeable increase in the reactor fuel campaign T (days) (Fig. 5b). The increase in ω_{f} also has no effect on the spectrum $\phi_{\text{Vn}}(E)$ of the reactor under study (Fig. 6). It should be noted that it is not possible with existing technologies to synthesize a fuel compact in which ω_{f} is more than 37.5%.

Therefore, for further research, we chose the type 1017 fuel pellet at $\omega_{\text{f}} = 18\%$. The 2221 spheres of the microfuel are used in the type 1017 fuel pellets with the dispersed phase fraction at the chosen $\omega_{\text{f}} = 18\%$. The fuel mass in this pellet is equal to 0.519×10^{-3} kg (Th, Pu)O_2, the full core loading = 600.6 kg, ^{232}Th = 246.24 kg, and ^{239}Pu = 231.47 kg.

According to the results obtained in WIMS, the reactor with this type of fuel pellets is capable of operating for 3110 effective days at the power $P = 60$ MWth. The neutron flux density in the core $\phi_{\text{Vn}}(E)$ is 8.14×10^{13} n cm^{-2} s^{-1}. There are 9.41% of the neutrons with energy E_{n} up to 4 eV, 35.57% of neutrons with E_{n} from 4 eV up to 183.2 keV, and 55.02% of neutrons with E_{n} from 183.2 keV to 10.5 MeV (Fig. 6b). In these conditions, (k_{eff}) is 1.24, $\rho_{\text{initial}} \approx 19.35\%$, and $(\text{d}\rho/\text{d}t) \approx 6.2 \times 10^{-3}$ %/days. The burn-up of ^{239}Pu is 81.3% ($\eta = N(0) - N(3110))/N(0)$), and the burn-up of ^{232}Th is 9.66%. The computation results of fuel isotopic composition evolution $N(t)$ are presented in Fig. 7 and in Table 1.

Additionally, the dependence of concentration changes of isotopes ^{231,233}Pa on time ^{231,233}N(t) was derived, and concentrations of ^{149}Sm and ^{135}Xe were analyzed. The data

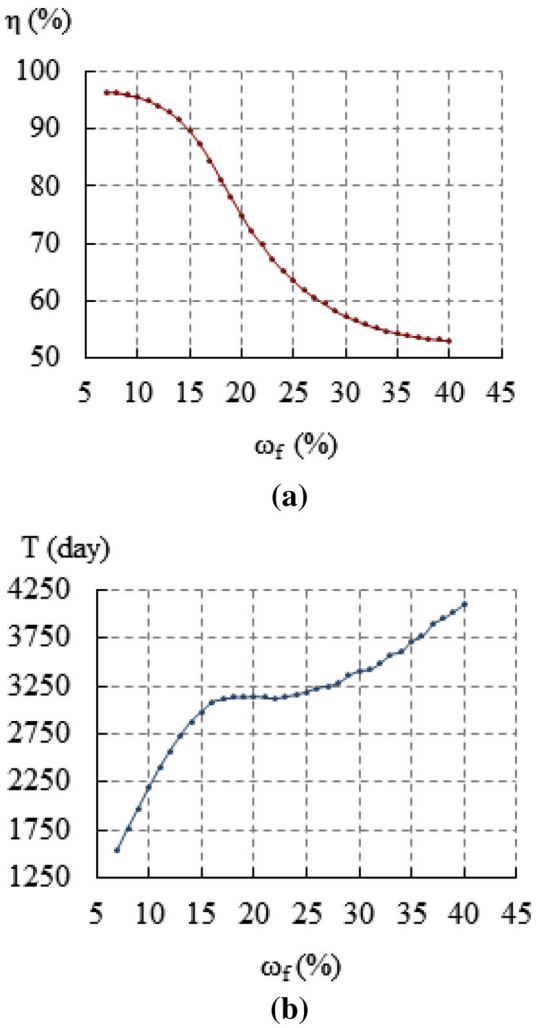

Fig. 5 Neutronic properties of the equivalent system: **a** dependence of $\eta(^{239}\text{Pu})$ on ω_{f}, **b** dependence of irradiation time T on ω_{f}

on ^{231,233}Pa, ^{233}U, ^{149}Sm, and ^{135}Xe concentrations allow the evaluation of the required intensity $I_{\text{n}}(t)$ of neutron emission from a thermonuclear reaction in a plasma column. By varying the percentage of D–T reactions in comparison with D–D reactions in the plasma column, one can change I_{n} within the range 10^{13}–2×10^{14} n cm^{-1} s^{-1}. That should provide the condition k_{eff} = constant during both the first days of operation of the facility and the whole fuel irradiation cycle.

The neutronic computation performed in WIMS-D5B was repeated in the program MCU5TPU [23]. The results of these computations are presented in Fig. 8. The code MCU5TPU was developed at the National Research Center Kurchatov Institute (Russia), and is used for simulation of particle transfer by the Monte-Carlo method in any reactor. MCU uses its own nuclear data bank, MCUDB50 [23].

If one creates a large initial reactivity excess ρ_{initial} (as demonstrated in Fig. 8), then a burnable absorber can

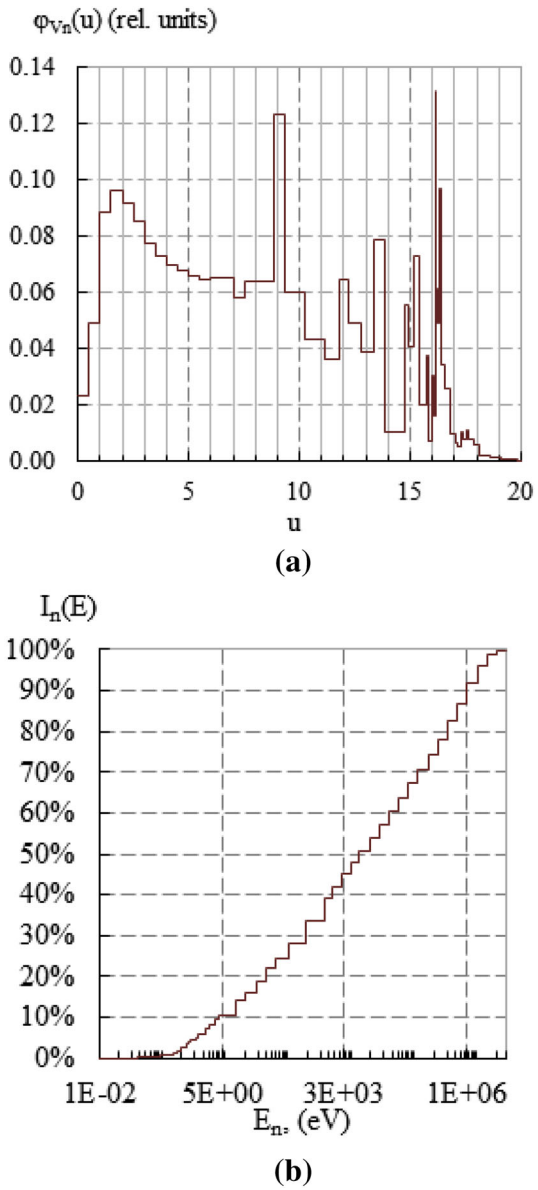

Fig. 6 The neutron spectrum in the reactor core: **a** normalized spectrum of the neutron flux; **b** integral distribution function of the neutrons over energy in the flux

compensate for this excess. For example, to compensate for the large $\rho_{initial}$ in the LWR and BN-type reactors, Gd_2O_3, Er_2O_3, and B_4C are used. In this case, daughter nuclides formed as a result of radiation capture reactions on ^{157}Gd, ^{167}Er, and ^{10}B do not have a significant impact regarding further neutronic processes in the core.

In solving the task of choosing the appropriate burnable absorber, it is of interest to search for nuclides, the daughter nuclides of which can have a favorable effect on the development of a self-supporting chain reaction. The authors of the works [24, 25] suggested using PaO_2 as a burnable absorber. A peculiar feature of isotope ^{231}Pa is

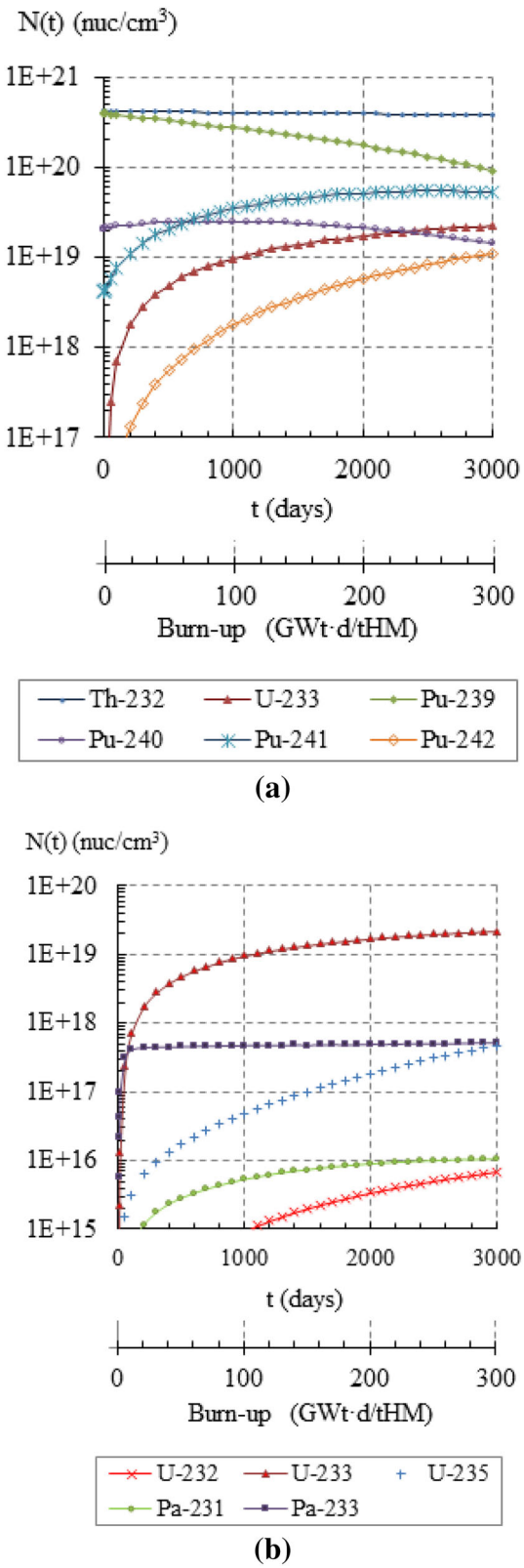

Fig. 7 Concentration evolution of the main minor actinides in HGTRU with time due to fuel burn-up (Color online)

Table 1 Mass content (wt%/mHM) of the minor actinides in the middle and at the end of the irradiation time t

Nuclide	Beginning of life	Medium of life	End of life
^{239}Pu	47%	26.54%	8.81%
^{240}Pu	2.5%	2.84%	2.35%
^{241}Pu	0.5%	5.39%	6.33%
^{242}Pu	–	0.42%	1.26%
^{232}Th	50%	47.82%	45.17%
^{232}U	–	0.00%	9.63E−04%
^{233}U	–	1.66%	2.70%
^{234}U	–	0.09%	0.28%
^{235}U	–	0.01%	0.07%
^{242}Cm	–	0.00%	0.13%
^{244}Cm	–	0.00%	0.20%
Burn-out (GWt × d/tHM)	0	145.5	304
t (days)	0	1500	3130

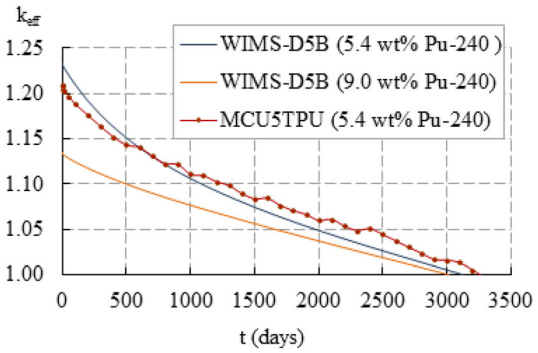

Fig. 8 Dependence of k_{eff} on the core operation time t in case of large initial reactivity excess (Color online)

that its transmutation leads to the formation of ^{232}U and ^{233}U, and isotope ^{233}U is a fissionable material. This means that isotope ^{231}Pa performs the functions of a burnable absorber and a source of a new fissionable material. However, ^{231}Pa production in the amounts required for implementation of the concept suggested in the work [24] is rather challenging. That said, ^{231}Pa can be effectively used in small amounts as a burnable absorber, for example, in a high-temperature reactor core.

In the work [25], it is suggested to use ^{240}Pu as a burnable material. In our case (Fig. 7), the presence of ^{240}Pu in the fuel composition results in significant accumulation of ^{241}Pu, which can be well fissioned by epithermal neutrons, and its nuclear concentration ^{241}N(t) exceeds the nuclear concentration of ^{233}U by more than 2.5 times across the whole fuel campaign. The computation showed that ^{241}Pu and ^{233}U specify the dependence type of $k_{\text{eff}}(t)$ and provide steady reactor operation for 8.5 years.

The proposed usage of ^{231}Pa becomes appropriate if we compare the dependency of absorption cross-sections $\sigma_{\text{abs}}(E)$ on the neutron energy E for traditional neutron absorbers with the dependency for ^{231}Pa (Fig. 9 and Table 2). It is seen in Fig. 9 (ENDF/B-VII.I) that the neutron absorption cross-section on the nuclei of ^{157}Gd, ^{167}Er, and ^{10}B for the neutron energy range 0.3–10^6 eV are on a level close to the absorption cross-section of the nuclei of ^{231}Pa.

If one examines Fig. 6b, one can come to the conclusion that about 91% of neutrons in the core of the reactor have energy more than 4 eV. The average value (E_{average}) on the neutron energy spectrum shown in Fig. 6a is 5.539×10^5 eV. The absorption cross-sections $\sigma_{\text{abs}}(E_{\text{average}})$ of the nuclei of absorbers and ^{231}Pa are presented in Table 2 for $\sigma_{\text{abs}}(E_{\text{average}})$. It can be seen that ^{231}Pa is likely to be a substitute for ^{10}B and some other traditional absorbers. The influence of ^{10}B on the neutronic properties of a reactor core with epithermal and fast neutron spectrum was analyzed by the authors in [1].

In the loading option discussed above (Fig. 8), the initial reactivity excess is compensated for by the isotope ^{240}Pu. Its content (wt%) in the fuel increased from 5.4 up to 9%; the content of ^{239}Pu decreased by 3.6%, correspondingly. The use of ^{240}Pu in HTGRU does not lead to any undesired increase in reactivity in the middle of the fuel cycle, as it happens in the core of the pressurized water reactor (PWR) [26]. Using ^{240}Pu, ρ_{initial} was reduced from 19.35 to 11.51%, and ($\mathrm{d}\rho/\mathrm{d}t$) decreased by a factor of 1.51. According to the concept suggested by the authors in the

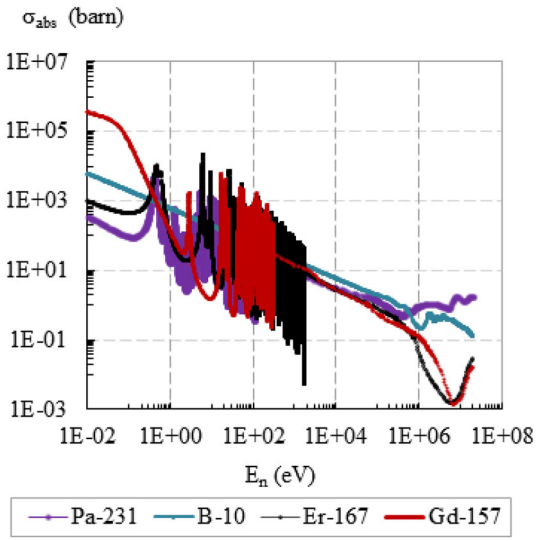

Fig. 9 Dependence of neutron absorption cross-sections of various isotopes on neutron energy (Color online)

Table 2 Neutron absorption cross-section for medium energy of the reactor energy spectrum

Nuclide	$\sigma_{abs}(E_{average})$ barn
^{231}Pa	0.742
^{10}B	0.656
^{167}Er	0.186
^{157}Gd	0.188
^{240}Pu	0.143

work [19], the core of HGTRU, the axial part of which is substituted by a long magnetic trap with high-temperature plasma, starts up from the subcritical state ($k_{eff} = 0.95$). To transfer the core into the subcritical state, it is enough to cover the surfaces of fuel pellets with a 13 μm thick layer of ZrB_2.

2.3 Computational model of the axial zone of the core; specific neutron yield of fusion plasma source

Currently, two types of neutron source for continuous operation in a fission–fusion hybrid energy system seem to be the most promising. The first type is an accelerator-driven system (ADS). This type is the most studied [27, 28]. In this work, we focus our studies on the second type—a neutron source based on fusion plasma in a long magnetic trap. The schematic drawing of the facility intended to study nuclei fuel properties in the operation of such a plasma neutron source is presented in Fig. 10 [19]. The axial zone of the reactor core is substituted for a cylindrical vacuum chamber that contains high-temperature plasma generating high-energy neutrons by D–D and/or D–T fusion reactions. To inject heating neutral beams into the plasma, a special chamber is attached to this cylindrical chamber. A magnetic field in these two adjoined vacuum chambers containing the plasma provides heat isolation of this plasma from the chamber walls in a radial direction. Heat isolation of the plasma along the magnetic field lines is provided by the multimirror sections of the magnetic field, which are adjacent to the ends of the two adjoined chambers of high-temperature plasma. The chamber for fusion neutron generation in the axial zone of the core has the required length of 3 m. The total length of the two adjoined chambers of high-temperature plasma is approximately 7 m. The total length of the whole facility is about 12 m.

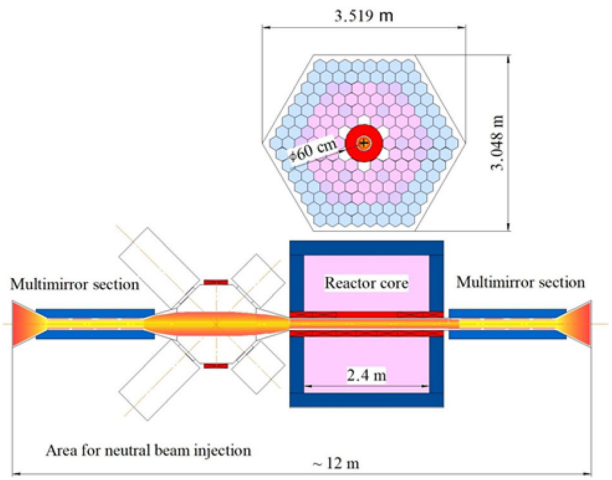

Fig. 10 Schematic of the facility containing the plasma neutron source to study the fuel properties in long-time operation of the reactor core (Color online)

Distribution of the magnetic field induction along the axis of the two adjoined chambers with high-energy ions (the length is approximately 7 m) was chosen in the paper [20] from considerations of the maximum neutron yield in the core plasma region upon the condition of good homogeneity of radial neutron flow. The choice of plasma parameters in the long magnetic trap was made according to the provided computation results. The results of the calculation [20] for the distribution along the z-axis of the specific neutron yield per linear centimeter of the plasma column in the case of D–D reaction is plotted in Fig. 11. A red bar located on the interval of z-coordinates from 200 to 500 cm marks the part of the column that is situated inside the reactor core. One can see in Fig. 11 that for the distribution of magnetic field and plasma column parameters chosen in [20], the specific neutron yield changed insignificantly in the plasma column part that was placed in the core. Nevertheless, non-homogeneity of plasma distribution along the z-axis may be taken into consideration in our simulations. As examples of the possibility to analyze various plasma distributions along the z-axis, the specific neutron yields of plasma neutron sources with cylindrical and conical shapes of the plasma column were analyzed.

In numerical simulation, it was considered that the plasma column is a volume source of monoenergetic

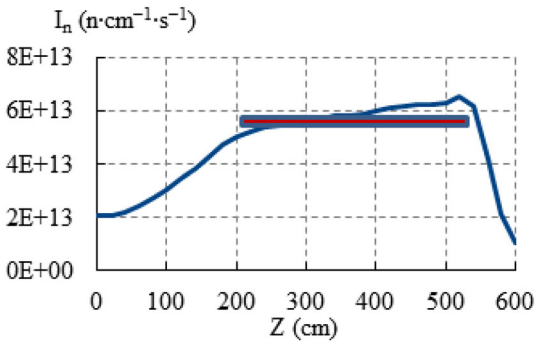

Fig. 11 Distribution of the specific neutron yield per linear centimeter of the plasma column in the case of D–D fusion reactions along the z-axis (the part of the column inside the reactor core is marked by the red line) (Color online)

neutrons with isotropic velocity distribution at the point of their origination.

In accordance with the results of the paper [20], injection of a 100 MW deuterium beam will produce high-energy sloshing ions with density up to $1.5 \times 10^{14}\,\mathrm{cm}^{-3}$. In this case, the specific emission of neutrons from a volume unit due to the D–D reaction is $1.76 \times 10^{12}\,\mathrm{n\,cm}^{-3}\,\mathrm{s}^{-1}$ in the core region, and the specific neutron yield rate is $6.00 \times 10^{13}\,\mathrm{n\,cm}^{-1}\,\mathrm{s}^{-1}$. The power of 2.45 MeV neutrons will be about 20 kW in the whole device and about 6 kW inside the core region. Two options are suggested to increase the neutron yield. The first is to add tritium and produce plasma with the percentage 50% D and 50% T isotopes. The simple estimation for this condition shows that neutrons with power of 14.1 MeV will generate up to 2.5–3 MW in the whole device and up to 0.8–0.9 MW inside the core region. If the injection power of neutral beams is reduced 10 times down to 10 MW, the power of D–T neutrons will decrease by approximately two orders of magnitude and will have values close to the basic D–D scenario. The second option is to improve plasma confinement by multimirror plugs, while the basic calculation assumes ordinary mirror configuration. This option could increase the neutron yield by several times, but its applicability is still contingent on experimental proofs.

We calculated a spatial neutron flux distribution $\phi_{\mathrm{Zn}}(z)$ over the z-axis for the external surface of the copper winding of the plasma neutron source for both cases: 50% T with 50% D, and 100% D at the same specific neutron yield $6.00 \times 10^{13}\,\mathrm{n\,cm}^{-1}\,\mathrm{s}^{-1}$. The neutron flux distributions for cylindrical and conical shapes of the plasma column were analyzed. The diameter of the cylindrical plasma column was 17 cm. For the conical column shape, its diameter decreased from 17 down to 13 cm over a length of 300 cm. As one can see in Fig. 10, a copper winding covers the external surface of the vacuum chamber. This copper winding has thickness 5 cm and is divided from the plasma column by the vacuum chamber wall, of thickness 4 mm. Considering the thickness of the winding, the external surface of the plasma neutron source has a diameter that varies from 22 to 18 cm for the conical plasma column shape. This diameter is 22 cm for the cylindrical shape. The neutron flux $\phi_{\mathrm{Sn}}(E)$ on the external surface of the copper winding was generated by usage of the program in the energy group structure ABBN-78 (of 28 energy neutron groups). Spatial neutron flux distribution $\phi_{\mathrm{n}}(z)$ with respect to the z-axis of the facility and its radius y was obtained by placing a computational grid with a size of 1000 by 1000 cells along the height z ($\phi_{\mathrm{Zn}}(z)$) and radius y ($\phi_{\mathrm{Yn}}(z)$) of the model.

The presented results were obtained in simulations performed using the programs MCNP5 (ENDF/B-VII.0) [29], Serpent 1.1.7 (ENDF/B-VII.0) [30], and PRIZMA (ENDF/B-VII.I) [31]. The study using the program PRIZMA was performed at the Zababakhin All-Russian Scientific Research Institute of Technical Physics (http://www.vniitf.ru/o-vniitf). The classic Monte-Carlo method was used to solve the task in the frame of the MCNP, Serpent, and PRIZMA applications. In the simulations, we considered the influence of copper coils on the propagation of the neutron fluxes in the volume of the stand. In accordance with the results of detailed computer simulations and the information about usage of copper conductors in fission reactors, we concluded that our magnetic field coils could be operated without being destroyed during the operation cycle of our fission–fusion stand.

3 Calculation data and discussion

The calculation data of the neutron flux density distribution $\phi_{\mathrm{Zn}}(z)$ on the external surface of the plasma neutron source for cylindrical (blue and green) and tapered (conic) plasma (red) are presented in Fig. 12 for both cases: 50% T with 50% D, and 100% D. For these calculations, we applied the computation model and program code in the frame of usage of MCNP5.

We used three different codes to calculate the data of the neutron flux normalized spectrum $\phi_{\mathrm{Sn}}(E)$ (the fraction of neutrons escaping in the direction of the core from 1 cm^2 of the facility side surface per second) on the external surface of the facility. As one can see in Fig. 13a, these three codes give almost identical results. The maximum discrepancy between MCNP5 and Serpent 1.1.7 is observed in the 26th energy group (that is, for neutrons in the energy range E_{n} from 6.5 to 10.5 MeV) and is -6.42%. The maximum discrepancy between MCNP5 and PRIZMA is $+3.35\%$ (the 26th energy group). The discrepancy in the calculation

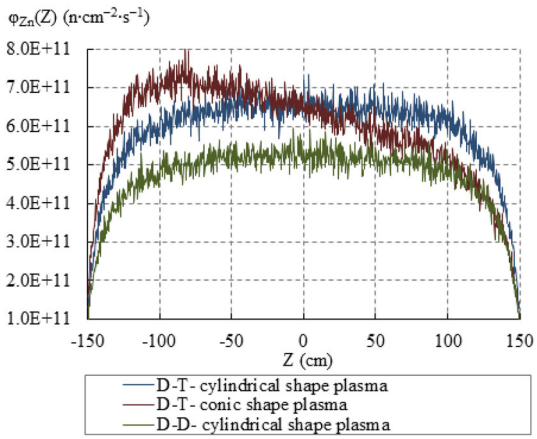

Fig. 12 Neutron flux density on the external surface of the plasma neutron source versus z-coordinate (Color online)

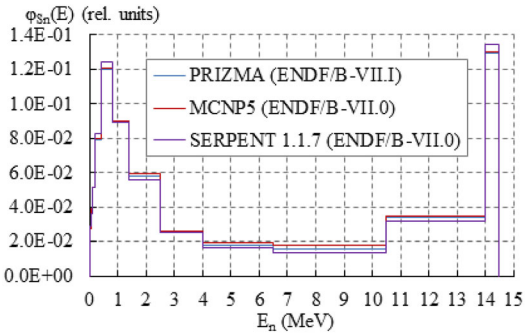

(a)

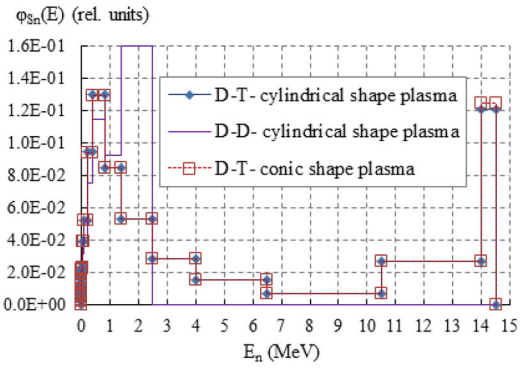

(b)

Fig. 13 Spectrum of the neutrons in the flux on the surface of the plasma neutron source (Color online)

data is conditioned by the use of the nuclear data from libraries of different revision and by the peculiarities of their preparation.

It can be seen in Fig. 11 that $\phi_{Zn}(z)$ greatly depends on the plasma column shape, but $\phi_{Sn}(E)$ differs significantly only in the 28th group (Fig. 13b) in the energy range of E_n from 14.0 to 14.5 MeV. Therefore, to determine the power distribution of D–T neutrons, it is possible not to consider plasma non-homogeneity and neutron flux in the radial direction.

The calculation data performed in Serpent (Fig. 14) showed that the probability density of neutron interactions of (*n, xn*) type was at a maximum in steel constructional elements and in inner layers of the copper solenoid (Fig. 14, red color). In the peripheral layers of the copper winding, the (*n*, 2*n*)-reaction is almost absent (Fig. 14, blue color).

If, however, the layer of BeO is placed on the external surface of the solenoid, D–T neutrons from the 23rd to 28th groups (neutrons with E_n from 2.5 to 14.5 MeV) contribute to the production of neutrons in the channel of (*n*, 2*n*) reactions on nuclei of isotope ^{9}Be.

In a fixed-source MCNP problem, the net multiplication M is defined to be unity plus the gain G_f in neutrons from fission, plus the gain G_x from no fission multiplicative

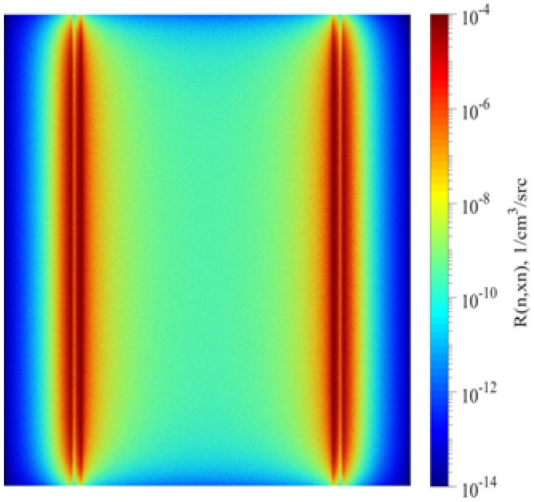

Fig. 14 Probability density of (*n*, 2*n*) reactions in constructional elements of the facility: longitudinal cross-section (Color online)

reactions. As the multiplication M in the facility is conditioned mainly by (*n*, 2*n*) reactions, in the case of D–T plasma $M = 1 + G_{n,2n}$. In the facility with D–T plasma of cylindrical and conical shape, M is equal to 1.2742 and 1.2728 (MCNP5), respectively. In addition, the contribution of (*n*, 2*n*)-reactions to multiplication is 21.3%. In the case of D–D plasma, M is 1.000 (MCNP5).

The total escape of D–D neutrons from the facility is 80.4%, while neutron escape from the side and end surfaces are 66.5 ($\phi_{Zn} = 6.67 \times 10^{12}\,\mathrm{n\,cm^{-2}\,s^{-1}}$ and 13.9% ($\phi_{Yn} = 1.39 \times 10^{13}\,\mathrm{n\,cm^{-2}\,s^{-1}}$), respectively.

The total escape of D–T neutrons from the facility is 98.5%, of which neutron escape from the sides and end surface is 83.6 ($\phi_{Zn} = 8.39 \times 10^{12}\,\mathrm{n\,cm^{-2}\,s^{-1}}$) and 14.9% ($\phi_{Yn} = 1.49 \times 10^{13}\,\mathrm{n\,cm^{-2}\,s^{-1}}$), respectively. It should also be mentioned that thorium in the first row of the assembly transmutes into ^{231}Pa under the influence of D–T neutrons from the 26th, 27th, and 28th groups due to (*n*, *xn*)-reactions. Therefore, the core provides extra neutrons and fissionable isotope ^{233}U.

To compare the neutron spectrum $\phi_{Sn}(E)$ (Fig. 13) with the spectrum $\phi_{Vn}(E)$ (Fig. 6) correctly, $\phi_{Sn}(E)$ was derived in the energy group structure WIMS69 (WIMS-D5B), and an additional neutron group with energy from 10.5 to 14.5 MeV (Fig. 14) was used. The neutron flux distribution functions $I_n(E_i) = \int_0^{Ei} \phi_n(E)\mathrm{d}E / \int_0^{\infty} \phi_n(E)\mathrm{d}E$ presented in Fig. 15 were derived in the same energy group structure as the functions $\phi_{Vn}(E)$ (Fig. 15, curve 1) and $\phi_{Sn}(E)$ (Fig. 15, curve 2).

In accordance calculations, neutrons escaping from the side surface of the facility (Fig. 16, curve 2) can be divided into four main group with different energy E_n. The percentages of these groups of neutrons are as follows:

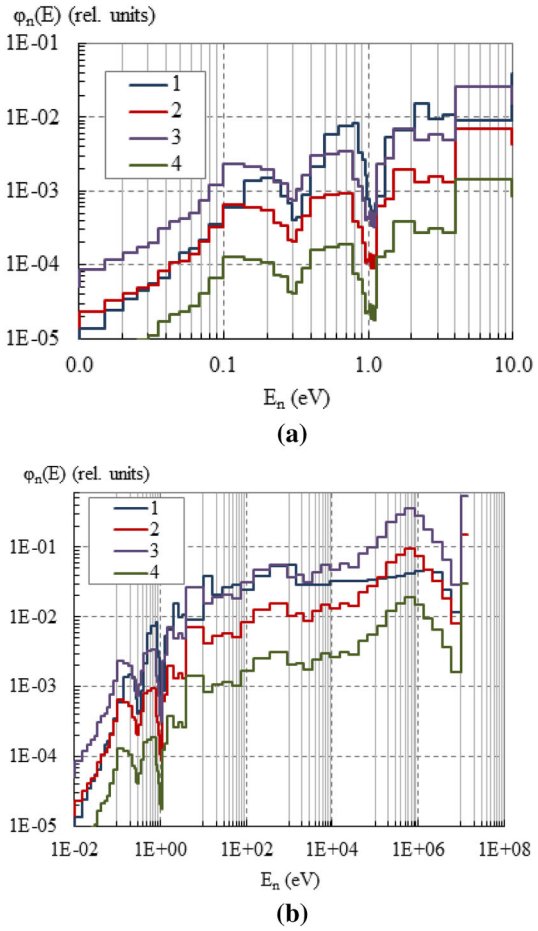

Fig. 15 Neutron flux energy spectrum: 1—normalized neutron flux energy spectrum $\phi_{Vn}(E)$ in the core; 2, 3, 4—normalized neutron flux energy spectrum $\phi_{Sn}(E)$ on the surface of the facility (Color online)

2.03%—E_n from zero to 4 eV (thermal neutrons), 30.19%—E_n from 4 eV to 183 keV (epithermal neutrons), 50.11%—E_n from 183 keV to 10.5 MeV, and 17.69%—E_n from 10.5 to 14.5 MeV (fast neutrons). In the reactor core

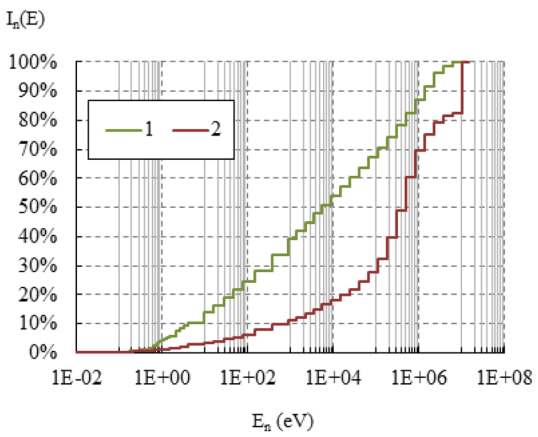

Fig. 16 Integrated energy distribution functions of neutron flux: 1—core; 2—side surface of the facility (Color online)

(Fig. 16, curve 1), there are 9.41% thermal neutrons, 35.57% epithermal, and 55.02% fast neutrons. For the data presented in Fig. 15, the specific neutron yield is $I_n = 6.0 \times 10^{13}\,\mathrm{n\,cm^{-1}\,s^{-1}}$ (Fig. 11).

To achieve the possibility of exactly correct usage of neutron emissions from the plasma source for studying neutronic and thermal–physical properties of thorium–plutonium fuel in the core of HGTRU, we have to achieve a specific neutron yield on the level $I_n = 1.8 \times 10^{14}\,\mathrm{n\,cm^{-1}\,s^{-1}}$ (Fig. 15, curve 3). This is three times large than the $6.0 \times 10^{13}\,\mathrm{n\,cm^{-1}\,s^{-1}}$ (Fig. 15, curve 2) that was already achieved in simulation for the D–D plasma column. This increase in neutron yield will be realized in the case of replacing a certain quantity of deuterium with tritium in the plasma column, without changing any other parameters of the plasma. In the case of the 50% T with 50% D in the plasma column with other plasma parameters unchanged, the specific neutron yield has to be 25 times greater.

4 Conclusion

Computer simulation of neutronic processes in the core of a high-temperature gas-cooled thorium reactor for 30 different options of core loadings was performed in the frame of our work. The quantity of fuel compact dispersion phase and the composition of fissionable nuclides were examined. Production of extra neutrons by the means of thermonuclear reactions occurring in high-temperature plasma and of (n, xn)-type reactions was analyzed. The possibility of applying a plasma D–T source of neutrons to modify the near-axial region of the HGTRU core was demonstrated. It was shown that the developed models and computer codes for description of the core and thermonuclear neutron source allow progression to a full-scale study aimed at creation of a thorium subcritical assembly with supply of extra neutrons from thermonuclear plasma through its confinement in the long magnetic trap.

Acknowledgements The authors thank Dr. S. Sinitsky for the schematic design of the copper winding in the region of the reactor core.

References

1. I.V. Shamanin, V.M. Grachev, S.V. Bedenko et al., Neutronic properties of high-temperature gas-cooled reactors with thorium fuel. Ann. Nucl. Energy **113**, 286–293 (2018). https://doi.org/10.1016/j.anucene.2017.11.045
2. S.V. Bedenko, N. Ghal-Eh, I.O. Lutsik, I.V. Shamanin, A fuel for generation IV nuclear energy system: isotopic composition and radiation characteristics. Appl. Radiat. Isot. **147**, 189–196 (2019). https://doi.org/10.1016/j.apradiso.2019.03.005
3. I.V. Shamanin, S.V. Bedenko, YuB Chertkov, Thorium-loaded low-power reactor installation operated with super-long fuel

residence time. Izvestiya Wysshikh Uchebnykh Zawedeniy, Yadernaya Energetika **2**, 121–132 (2016). **(in Russia)**
4. Innovative nuclear systems of the VI generation, see https://world-nuclear.org/info/inf33.html. Accessed 04 April 2019
5. V. Kuznetsov, Options for small and medium sized reactors to overcome loss of economies of scale and incorporate increased proliferation resistance and energy security. Prog. Nucl. Energy **50**(2–6), 242–250 (2008). https://doi.org/10.1016/j.pnucene.2007.11.006
6. M.K. Rowinski, T.J. White, J. Zhao, Small and medium sized reactors: a review of technology. Renew. Sustain. Energy Rev. **44**, 643–656 (2015). https://doi.org/10.1016/j.rser.2015.01.006
7. U.E. Humphrey, M.U. Khandaker, Viability of thorium-based nuclear fuel cycle for the next generation nuclear reactor: issues and prospects. Renew. Sustain. Energy Rev. **97**, 259–275 (2018). https://doi.org/10.1016/j.rser.2018.08.019
8. T. Abram, S. Ion, Generation-IV nuclear power: a review of the state of the science. Energy Policy **36**(12), 4323–4330 (2008). https://doi.org/10.1016/j.enpol.2008.09.05
9. D.Y. Cui, S.P. Xia, X.X. Li et al., Transition toward thorium fuel cycle in a molten salt reactor by using plutonium. Nucl. Sci. Technol. **28**, 152 (2017). https://doi.org/10.1007/s41365-017-0303-y
10. D.A. Petti, R.R. Hobbins, P. Lowry, H. Gougar, Representative source terms and the influence of reactor attributes on functional containment in modular high-temperature gas-cooled reactors. Nucl. Technol. **184**(2), 181–197 (2013). https://doi.org/10.13182/NT184-181
11. A. Talamo, W. Gudowski, Adapting the deep burn in-core fuel management strategy for the gas turbine—modular helium reactor to a uranium–thorium fuel. Ann. Nucl. Energy **32**(16), 1750–1781 (2005). https://doi.org/10.1016/j.anucene.2005.07.002
12. H. Chang, Y. Yang, X. Jing, Y. Xu, Thorium-based fuel cycles in the modular high temperature reactor. Tsinghua Sci. Technol. **11**(6), 731–738 (2016). https://doi.org/10.1016/S1007-0214(06)70257-7
13. H. Nickel, H. Nabielek, G. Pott, A.W. Mehner, Long time experience with the development of HTR fuel elements in Germany. Nucl. Eng. Des. **217**(1–2), 141–151 (2002). https://doi.org/10.1016/S0029-5493(02)00128-0
14. C.Y. Zou, C.Z. Cai, C.G. Yu, J.H. Wu, J.G. Chen, Transition to thorium fuel cycle for TMSR. Nucl. Eng. Des. **330**, 420–428 (2018). https://doi.org/10.1016/j.nucengdes.2018.01.033
15. Innovative nuclear systems of the VI generation (Akademik Lomonosov-1, 2), see www.okbm.nnov.ru/upload/iblock/456/45621ca6723f2345078c93b06b36c7e2.pdf. Accessed 11 Oct 2018. **(in Russia)**
16. High Temperature Gas Reactor: SHIDAO BAY-1 https://prisweb.iaea.org/PRIS/CountryStatistics/ReactorDetails.aspx?current=957. Accessed 11 Oct 2018
17. The project for constructing a Small Modular Reactor (Idaho National Laboratory), see https://inl.gov/article/frequently-asked-questions/. Accessed 04 April 2019
18. US Department of Energy, the project for constructing a High Temperature Gas Reactor, see https://world-nuclear-news.org/Articles/Triso-project-clears-first-phase-of-loan-guarantee. Accessed 04 April 2019
19. A.V. Arzhannikov, A.B. Anikeev, A.D. Beklemishev et al., Subcritical assembly with thermonuclear neutron source as device for studies of neutron-physical characteristics of thorium fuel, in AIP Conference Proceedings, **1771**, (2016). https://doi.org/10.1063/1.4964246
20. D.V. Yurov, V.V. Prikhodko, YuA Tsidulko, Nonstationary model of an axisymmetric mirror trap with nonequilibrium plasma. Plasma Phys. Rep. **42**(3), 210–225 (2016). https://doi.org/10.1134/S1063780X16030090
21. P.A. Bagryansky, A.A. Ivanov, E.P. Kruglyakov et al., Gas dynamic trap as high power 14 MeV neutron source. Fusion Eng. Des. **70**(1), 13–33 (2004). https://doi.org/10.1016/j.fusengdes.2003.08.002
22. A. Pazirandeh, S. Ghaseminejad, M. Ghaseminejad, Effects of various spacer grid modeling on the neutronic parameters of the VVER-1000 reactor. Ann. Nucl. Energy **38**, 1978–1986 (2011). https://doi.org/10.1016/j.anucene.2011.04.020
23. MCU Project. Monte Carlo modelling of particle transport, see https://mcuproject.ru/rabout.html. Accessed 07 Oct 2018. **(in Russia)**
24. G.G. Kulikov, E.G. Kulikov, A.N. Shmelev et al., Protactinium-231—new burnable neutron absorber. Izvestiya Wysshikh Uchebnykh Zawedeniy, Yadernaya Energetika. **3**, 195–204 (2017). **(in Russia)**
25. A.N. Shmelev, G.G. Kulikov, V.A. Kurnaev et al., Hybrid fusion–fission reactor with a thorium blanket: its potential in the fuel cycle of nuclear reactors. Phys. At. Nuclei **78**(10), 1100–1111 (2015). https://doi.org/10.1134/S1063778815100117
26. A. Hussain, C. Xinrong, Small PWR core design with coated particle based fuel with a novel composition. Prog. Nucl. Energy **52**(6), 531–535 (2010). https://doi.org/10.1016/j.pnucene.2010.02.003
27. Neutron Source (Oak Ridge National Laboratory), see https://neutrons.ornl.gov/sns. Accessed 11 Oct 2019
28. J. Knastera, F. Arbeiter, P. Carac et al., IFMIF, the European–Japanese efforts under the Broader Approach agreement towards a Li(d, xn) neutron source: current status and future options. Nucl. Mater. Energy **9**, 46–54 (2016). https://doi.org/10.1016/j.nme.2016.04.012
29. F.B. Brown, The MCNP5 Random Number Generator, LA-UR-07-7961 (2007)
30. J. Leppanen, M. Pus, T. Viitanen et al., The Serpent Monte Carlo code: status, development and applications in 2013. Ann. Nucl. Energy **82**, 142–150 (2015). https://doi.org/10.1016/j.anucene.2014.08.024
31. Y.Z. Kandiev, E.A. Kashaeva, K.E. Khatuntsev et al., PRIZMA status. Ann. Nucl. Energy **82**, 116–120 (2015). https://doi.org/10.1016/j.anucene.2014.09.006